





Article

Photocatalytic Denitrification of Nitrate Using Fe-TiO₂-Coated Clay Filters

Tanveer A. Gadhi ^{1,*}, Imtiaz Ali Bhurt ¹, Tayyab A. Qureshi ¹ , Imran Ali ^{2,*} , Anira Latif ¹ , Rasool Bux Mahar ¹, Najeebullah Channa ³ and Barbara Bonelli ³ 

¹ U.S. Pakistan Center for Advanced Studies in Water (USPCASW), Mehran University of Engineering and Technology, Jamshoro 76062, Pakistan

² Department of Environmental Sciences, Sindh Madressatul Islam University, Aiwan-e-Tijarat Road, Karachi 74000, Pakistan

³ Department of Applied Science and Technology, Politecnico di Torino, Corso Duca degli Abruzzi 24, 10129 Torino, Italy

* Correspondence: tanveer.uspcasw@faculty.muett.edu.pk (T.A.G.); imranali@hanyang.ac.kr (I.A.)

Abstract: In this work, 3D-structured clay filters were prepared and coated with iron-doped titanium dioxide (Fe-TiO₂) using 3D printing and sol-gel soaking and calcination techniques. Three-dimensional printing was employed to mold and shape the clay filters before annealing. The coated and uncoated filters were characterized for different properties, i.e., morphology, optical properties, and crystalline structure, using field emission scanning electron microscopy (FESEM), energy-dispersive X-ray spectroscopy (EDS), UV/Vis diffused reflectance spectroscopy (DRS), and X-ray diffraction (XRD). The FESEM images show uniform coatings of round-shaped Fe-TiO₂ on the tiny pore of the clay filter. The optical energy band gap of the obtained coating was around 2.8 eV, estimated by Tauc's plot, compared with 3.2 eV of pristine anatase TiO₂. The XRD spectra data processed through XRD software revealed the coatings of TiO₂ on the filter surface with the obtained phase of anatase. The photocatalytic performance of bare and coated filters was initially tested for the degradation of indigo carmine (IC) dye and the obtained results suggested the photocatalytic degradation of IC dye by the Fe-TiO₂ clay filter compared with the bare filter. Afterward, the denitrification of nitrate NO₃ at various concentrations was performed using Fe-TiO₂-coated clay filters and analyzing the total nitrogen (TN) analysis and reduction of NO₃ to nitrite (NO₂[−]), nitrogen monoxide (NO), and nitrogen gas (N₂). The TN analysis revealed up to 81% denitrification efficiency of the 30 ppm NO₃ solution with the photocatalytic response of the Fe-TiO₂-coated filter. The results revealed that the Fe-TiO₂-coated clay filter has a high potential for denitrification applications under natural sunlight.

Keywords: photocatalysis; denitrification; iron; TiO₂; wastewater; 3D printing



Citation: Gadhi, T.A.; Bhurt, I.A.; Qureshi, T.A.; Ali, I.; Latif, A.; Mahar, R.B.; Channa, N.; Bonelli, B. Photocatalytic Denitrification of Nitrate Using Fe-TiO₂-Coated Clay Filters. *Catalysts* **2023**, *13*, 729. <https://doi.org/10.3390/catal13040729>

Academic Editor: Da-Ren Hang

Received: 26 February 2023

Revised: 4 April 2023

Accepted: 11 April 2023

Published: 12 April 2023



Copyright: © 2023 by the authors. Licensee MDPI, Basel, Switzerland. This article is an open access article distributed under the terms and conditions of the Creative Commons Attribution (CC BY) license (<https://creativecommons.org/licenses/by/4.0/>).

1. Introduction

The growing population demands industrial and agricultural growth for their survival, but such development has placed the environment under serious threat [1]. The release of untreated wastewater, including agricultural runoff (containing synthetic fertilizers and pesticides), industrial effluents (containing different chemicals), and sewage sludge, has led to the growth of many nutrient-rich micropollutants and pathogens in ground and surface water tables [2,3]. However, the quality of these resources is threatened by various anthropogenic activities that are harmful to the overall ecosystem.

Water pollution is a global ecological problem [4]. It adversely impacts daily human life and the natural ecosystem [5]. Excessive concentration of pollutants begets multiple diseases thanks to their toxicity and harmful nature [6]. Many studies have identified numerous nutrient-rich organic and inorganic pollutants, including nitrate, and found their excessive presence in different water resources, rapidly depleting their quality.

Nitrogen-containing compounds are considered one of the main hazardous pollutants, creating a tough emerging threat to the natural environment [7]. Nitrate (NO_3) is the stable, oxidized, and soluble form of nitrogen [4]. Various sources contribute to nitrate pollution, such as sewage, agricultural runoff, food processing and manufacturing, and livestock waste [8,9]. The removal of nitrate is of special interest because nitrogen is mainly behind the eutrophication and algal blooming of receiving water. It has harmful impacts on aquatic species and causes waterborne diseases that harm human health [10].

The unprecedented increases in the human population and industry growth have increased the demand for high-quality water resources [11]. Water scholars have come up with advanced ideas to find feasible alternatives for dealing with nitrate. Several efforts have been made to optimize the reduction and removal of nitrate.

Conventional techniques of nitrate removal, i.e., biological denitrification, ion exchange, and reverse osmosis, have been observed as energy-intensive techniques and could lead to secondary pollutants and more intense forms of nitrogen [12]. The main concern is reducing nitrate into less harmful compounds in wastewater or its ionic separation from the treating water. Many challenges in conventional treatment processes were encountered, such as the low-temperature effect; sensitivity to dissolved oxygen effect; high concentration build, helping in the separated stream; accumulation of nitrite ions; and so on.

In recent years, the applications of photocatalytic approaches have led to the development of the oxidative degradation procedure [13] thanks to the unique features of photocatalysis, prepared by a semiconductor photocatalyst i.e., TiO_2 . Photocatalysis can be used as an alternative for treating organically contaminated water. It employs very low-energy UV-A light, where catalysts can be reused, and additional oxidants are unnecessary [10–14]. TiO_2 has been considered the more stable photocatalyst thanks to its unique features, such as being cost-effective and harmless [15].

The TiO_2 and various doped TiO_2 materials have been extensively studied for potential applications in the production of hydrogen, cleansing, the synthesis of organics, and disinfection processes [12]. However, the large band gap (3.2 eV) is the main disadvantage of TiO_2 , meaning that activation can only occur upon irradiations with photons of light in the UV domain. This limits practical efficiency in solar applications [16,17]. Therefore, the efficiency of solar for TiO_2 under solar irradiations can be achieved through TiO_2 modification to facilitate visible light absorption [17]. Some methods are being developed for TiO_2 as a visible-light-active photocatalyst. Doping of Fe is a good tool for improving the photocatalytic properties of TiO_2 to be active under sunlight [18,19].

Using powder-form photocatalysts is efficient, but their recovery and reuse are challenging [20]. Various materials are being used as photocatalyst supporting media, of which clay is widely used thanks to its high porosity, surface area, and easier availability. Naturally occurring clay has low to median anion absorption capacity, facilitating physical and chemical modification to improve its surface properties [21]. Thanks to their low cost, high sorption properties, and potential for ion exchange, clay materials are considered robust adsorbents. Clay filters have good strength and permeability, are chemically inert, and resist high temperatures. Clay has potential applications in water and wastewater treatment [22,23].

Recently, 3D printing technology has attracted researchers' attention to synthesize 3D structured and porous filters as supporting media for the photocatalyst's various water treatment applications [24,25]. The coatings of nanoparticles on a 3D clay filter make the photocatalyst strong and interactive and support ion exchange reactions [26,27]. Some preparation methods for coating TiO_2 on supported 3D clay filters have been reported by various studies [28]. Sol-gel is one of the most versatile methods for synthesizing modified titanium dioxide particles such as Fe- TiO_2 [29]. It permits fine control of the material's nanostructure, morphology, and porosity and requires relatively simple equipment [30].

In this study, our previously reported innovative method of preparing standard 3D structured clay filters was employed as a photocatalyst supporting media [22]. Fe- TiO_2

particles were coated on the surface of a 3D-structured clay filter using the sol–gel soaking method. The selection of Fe-TiO₂ for coating on 3D-structured clay filters was based on our previous work, where Fe doping enhanced the photocatalytic properties under visible light. The photocatalytic activity of the bare and Fe-TiO₂ deposited clay filters was confirmed initially for the degradation of the indigo carmine (IC) dye under natural sunlight [31]. After validating the photocatalytic performance of Fe-TiO₂ against the removal of IC, the denitrification of NO₃ was experimented with to explore its photocatalytic reduction and mineralization into nitrogen gas. The obtained results showed promising denitrification potential of NO₃ by employing the Fe-TiO₂-deposited clay filters.

2. Results and Discussion

2.1. Characterization of the Clay Filters

Bare and Fe-TiO₂-coated clay filters were characterized for UV/Vis spectroscopy, XRD, EDS, and FESEM to evaluate their optical properties, phase and crystalline structure, elemental analysis, and morphology, respectively.

2.1.1. XRD

The X'PERT High Score software was used to analyze the XRD peaks of bare and Fe-TiO₂ clay filters, and the obtained XRD patterns are shown in Figure 1A. A broad peak in the 18–24° region is ascribed to clay. Meanwhile, in the case of the coated filter, the obtained major XRD peaks at 2θ, 25.281, 34.14, 37.934, 48.374, 53.888, and 55.296°, are ascribed to anatase TiO₂ (reference PDF card: 00-001-0562) [19]. The analyzed XRD patterns of the coated filter confirmed the integration of Fe-TiO₂ particles on the surface of the clay filter. The presence of any peak associated with Fe or its metalloid was not observed in the coated filter XRD spectra; probably being low in concentration, its peaks were suppressed/distorted by the background signals of the clay.

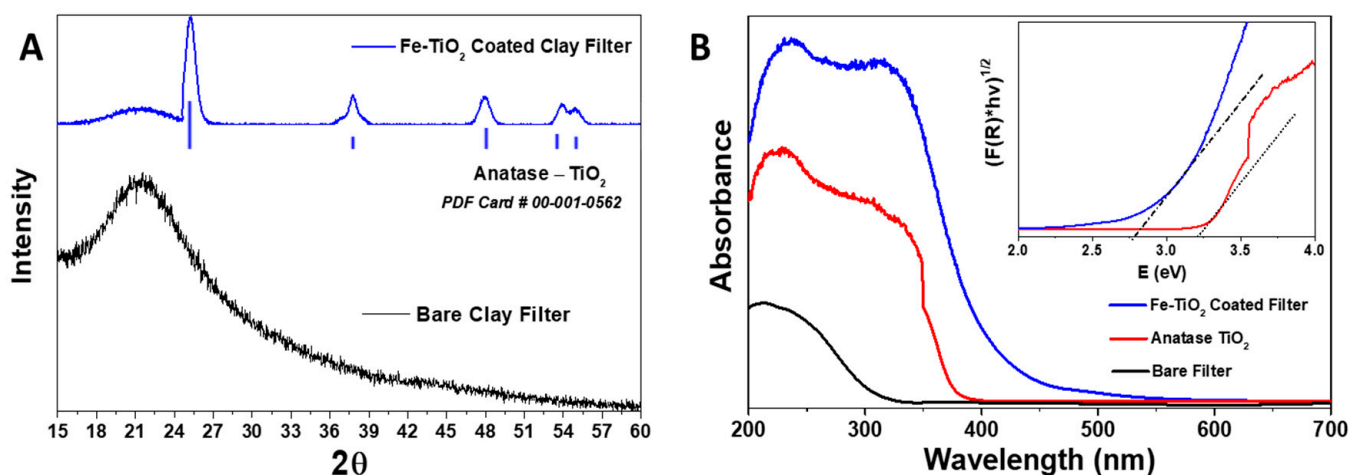


Figure 1. (A) XRD patterns of bare and Fe-TiO₂-coated clay filters and (B) UV/Vis DRS spectra of bare and Fe-TiO₂-coated clay filter and anatase TiO₂ (without Fe); inset, Tauc plot of the coated filter and anatase TiO₂ (without Fe) with an estimated energy band gap.

2.1.2. UV/Vis Spectroscopy

The UV/Vis DRS spectra of the bare and Fe-TiO₂-coated filters and anatase TiO₂ (without Fe addition) are shown in Figure 1B. The bare filter has absorbance below the 300 nm region, while the coated filter shows typical TiO₂ optical absorption spectra in the region between 300 and 350 nm and further stretching from 350 to 450 nm i.e., owing to 2.5% Fe addition [19]. The addition of Fe revealed the photo-absorption and solar activation potential of TiO₂ compared with the anatase TiO₂ (without Fe). The UV/Vis spectra of the annealed Fe-TiO₂ clay filter were also compared to spectra for TiO₂ reported in [29], and

the comparison results confirmed that doping of Fe has extended the absorbance of TiO_2 , which could facilitate the transition of visible light electrons from the valence band (VB) to the conduction band (CB) [19,29]. The estimated band gap of Fe-TiO_2 is around 2.8 eV, i.e., using the Tauc's plot (inset Figure 1B), lesser than that of TiO_2 without Fe addition, i.e., 3.2 eV.

2.1.3. FESEM Morphology

Figure 2A,B show the bare filter's FESEM images and Figure 2C–F show FESEM images of the Fe-TiO_2 -coated clay filter at different magnifications. The FESEM images of the bare filter show the rough and irregular clay particles with tiny pores, i.e., enabled after high-temperature annealing. Meanwhile, Figure 2C–F shows that the round-shaped Fe-TiO_2 particles are uniformly coated and filled on the rough and pore channels of the clay filter. The estimated average size of the round-shaped Fe-TiO_2 particles was in the range of 110 nm–280 nm. The EDS elemental analysis of the spotted tiny pores of the Fe-TiO_2 -coated filter is shown in Figure 2G, which confirmed the presence of Ti and Fe along with other elements, i.e., Si, O, and C.

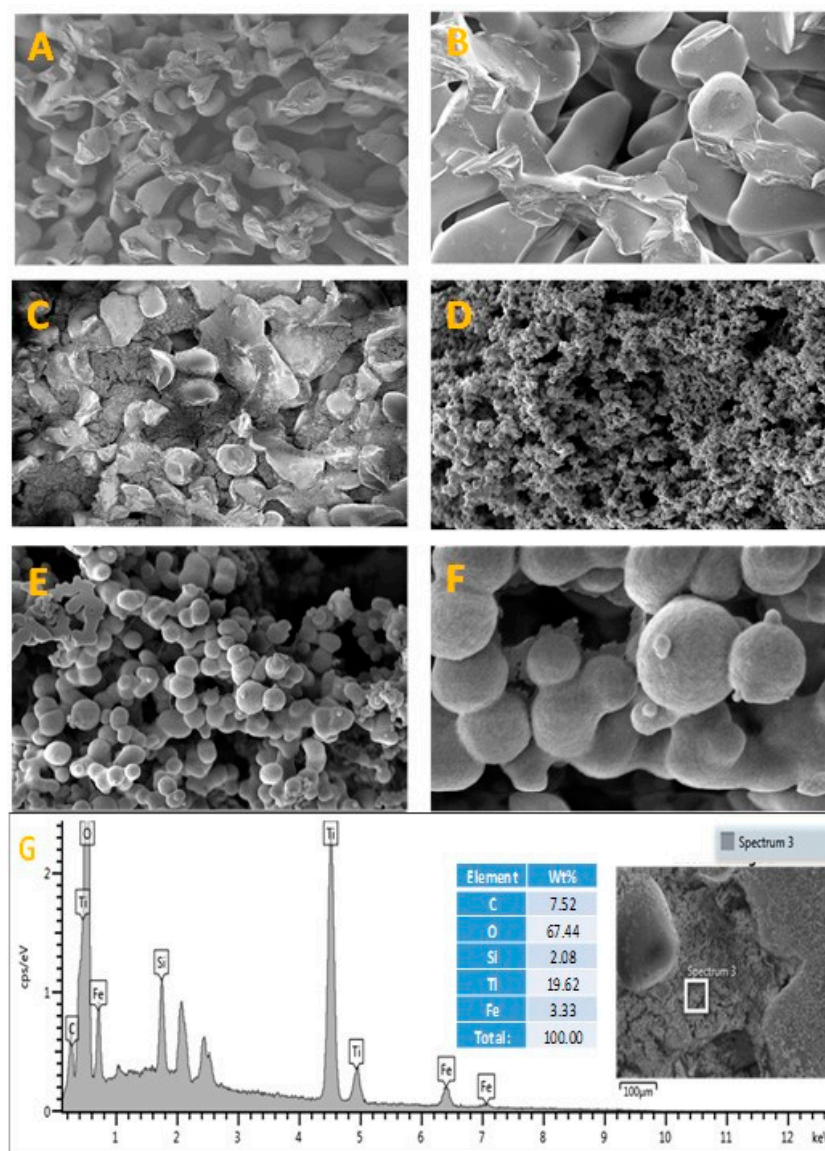


Figure 2. FESEM images of the (A,B) annealed bare clay filter and (C–F) Fe-TiO_2 -coated clay filter at different magnifications, and (G) EDS spectra along with weight % of elements.

2.2. Photocatalytic Evaluation of IC Dye

The results of IC dye degradation were analyzed through spectrophotometer UV/Vis absorbance spectra for control (only sunlight), bare, and Fe-TiO₂ filters. The obtained kinetic results in Figure 3B revealed the photocatalytic decomposition of IC dye compared with bare and control test results by achieving the relative concentration (C/C_0) decrease to almost 0.1 after 180 min of treatment. The UV–Vis absorbance spectra of the IC dye versus irradiation at a different time and with an Fe-TiO₂-coated filter (Figure 3A) showed the decreased trend of the main absorbance peak at 610 nm, and the spectral changes in the UV region confirmed the degradation and formation of secondary intermediate compounds, i.e., Isatin sulfonic acid and 2-amine-5-sulfo-benzoic acid [32,33]. The TOC analysis of the IC dye solution i.e., before and after the photocatalytic test with the coated filter, showed a decrease of 42% of organic carbon and mineralization of the IC dye. This was probably achieved by the radical species originating from the Fe-TiO₂-coated particles on the clay surface [22,34]. The acquired photocatalytic results confirmed the photocatalytic response of coated clay filters and the further advantage of doping Fe with TiO₂ for improved performance under solar light.

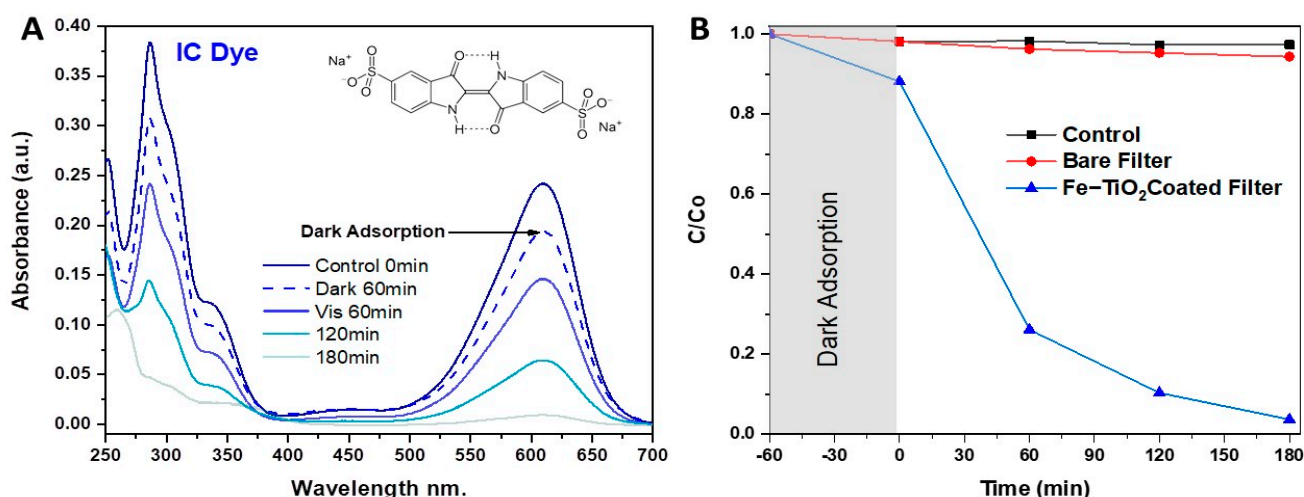


Figure 3. (A) The UV–Vis absorbance spectra of indigo carmine (IC) dye vs. irradiation at a different time and with the Fe-TiO₂-coated filter; (B) relative concentrations (C/C_0) of the IC with the control, bare, and coated filter.

2.3. Photocatalytic Denitrification Evaluation

The photocatalytic denitrification for NO₃ was tested with and without bare and coated filters for only a 30 ppm concentration of NO₃ under natural sunlight irradiation. The TN value was analyzed to evaluate the photocatalytic reduction of NO₃ and its transformation into N₂ for all experimental conditions. Further, the same test was conducted for 50 ppm and 100 ppm NO₃ using only the coated filter. Figure 4A shows the varying TN relative concentrations of the Fe-TiO₂ clay filter compared with the control solution and bare clay filter under sunlight irradiation. The results of the bare clay filter and control sample (Figure 4A) showed a slight decrease in the relative concentration of TN, then the concentrations remained unchanged, while the NO₃ concentrations underwent a photocatalytic reduction owing to the photocatalytic effect of Fe-TiO₂.

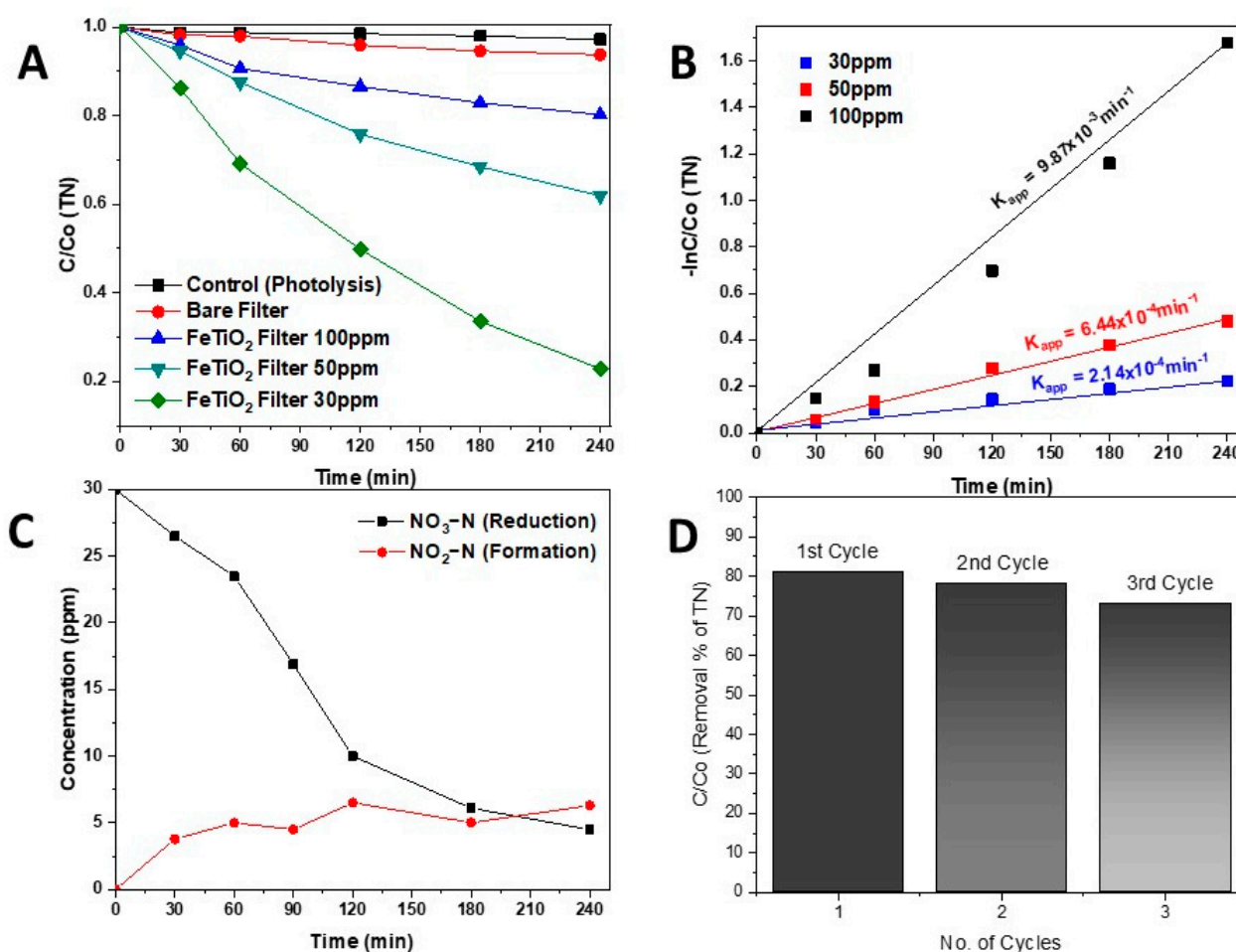


Figure 4. (A) Relative concentration of TN reduction of 30, 50, and 100 ppm using control, bare, and Fe-TiO₂ clay filters; (B) Kinetic curves with estimated kinetic apparent constant (K_{app}) values at concentrations using Fe-TiO₂ clay filters; (C) NO₃ reduction and nitrite (NO₂[−]) formation kinetics at a concentration of 30 ppm NO₃; and (D) cyclic stability performance of Fe-TiO₂ clay filters at a concentration of 30 ppm NO₃.

The photocatalytic selectivity towards nitrogen was calculated based on varying concentrations of TN of the treated solution [12,35]. The denitrification efficiency of the Fe-TiO₂ clay filter with varying NO₃ concentrations, the results of which are shown in Figure 4A, revealed 81% efficiency of 30 ppm, while the increasing load of nitrate nitrogen reduced denitrification, as 39% and 28% denitrification efficiencies were observed at 50 ppm and 100 ppm of TN, respectively.

The analyzed reduction of relative concentrations (C/C_0) using a Fe-TiO₂ clay filter revealed the effective reduction of 30 ppm compared with that of 50 ppm and 100 ppm. Figure 4B shows the TN kinetic curves with estimated kinetic apparent constant (K_{app}) values at 30, 50, and 100 ppm concentrations using the Fe-TiO₂ clay filter. The estimated K_{app} values were as follows: 9.87×10^{-3} , 6.44×10^{-3} , and $2.14 \times 10^{-3} \text{ min}^{-1}$ for 30, 50, and 100 ppm NO₃ concentrations, respectively. The decrease in kinetic removal of TN at a high loading of NO₃ could be related to the limited availability of radical species for the targeted reduction of NO₃.

The denitrification path was verified by measuring NO₃ reduction and NO₂[−] (nitrite) formation in the treated solutions. Figure 4C shows the reduction of NO₃ concentrations and transformation into nitrite ions before eventually mineralizing into N₂. The NO₂ formation was observed during the reduction of 30 ppm of NO₃ concentration (Figure 4C), as the initial sample indicated zero NO₂, but, after 30 min irradiation exposure with the

presence of the Fe-TiO₂ clay filter, 3 ppm of NO₂ was observed. Similarly, a maximum NO₂ concentration of around 6 ppm was observed at 240 min, with subsequent reduction of NO₃. This path indicated the reduction of NO₃ by radical species of Fe-TiO₂, transforming first in NO₂, later probably in NO, and finally in N₂, i.e., by comparing the TN reduction in Figure 4A and NO₂ formation in Figure 4C. The cyclic stability of the Fe-TiO₂ clay filters was tested for three repeated cycles of photocatalytic tests of the same filters for the denitrification of 30 ppm NO₃ solution. The obtained results are shown in Figure 4D, which revealed a slight decrease in the photocatalytic performance of Fe-TiO₂ clay filters from 81% to 72% in the third cycle and suggested the consideration of further improvements to be made in Fe-TiO₂ coating methods and mode of applications.

2.4. Photocatalytic Mechanism

The results suggested the improved efficiency of the Fe-TiO₂ clay filter in reducing the TN concentration under natural sunlight. Based on the photocatalytic properties of Fe-TiO₂ and the supporting information from the available literature studies [10,14,16], the possible mechanism of photocatalytic NO₃ reduction is shown in Figure 5. From the photocatalytic results obtained with the degradation of IC and nitrate reduction, it could be summarized that Fe-TiO₂ coated on a clay filter was photo-excited under exposure to sunlight and released hydroxyl (OH[•]) and superoxide (O^{•−}) radicals across the clay filter. Moreover, these radicals could have attacked NO₃ for its photocatalytic reduction into NO₂ and NO, and finally into N₂ gas, as reported [36,37]. The nitrate in soluble form could be denitrified by microbial denitrification. However, this study and other supported studies revealed that photocatalytic denitrification could be achieved using the reduction potential of photocatalysts [36,37]. The strong interaction between Fe-TiO₂ and rough and porous clay improved kinetics and supported the interface to adsorb NO₃ for its targeted reduction. The previous work of photocatalytic denitrification reported that the formation of intermediate counter products of nitrous oxide (N₂O), ammonia (NH₃), and ammonium (NH₄⁺) could occur owing to redox reactions that need to be analyzed to avoid the path of the photocatalytic denitrification in the formation of toxic compounds or gases.

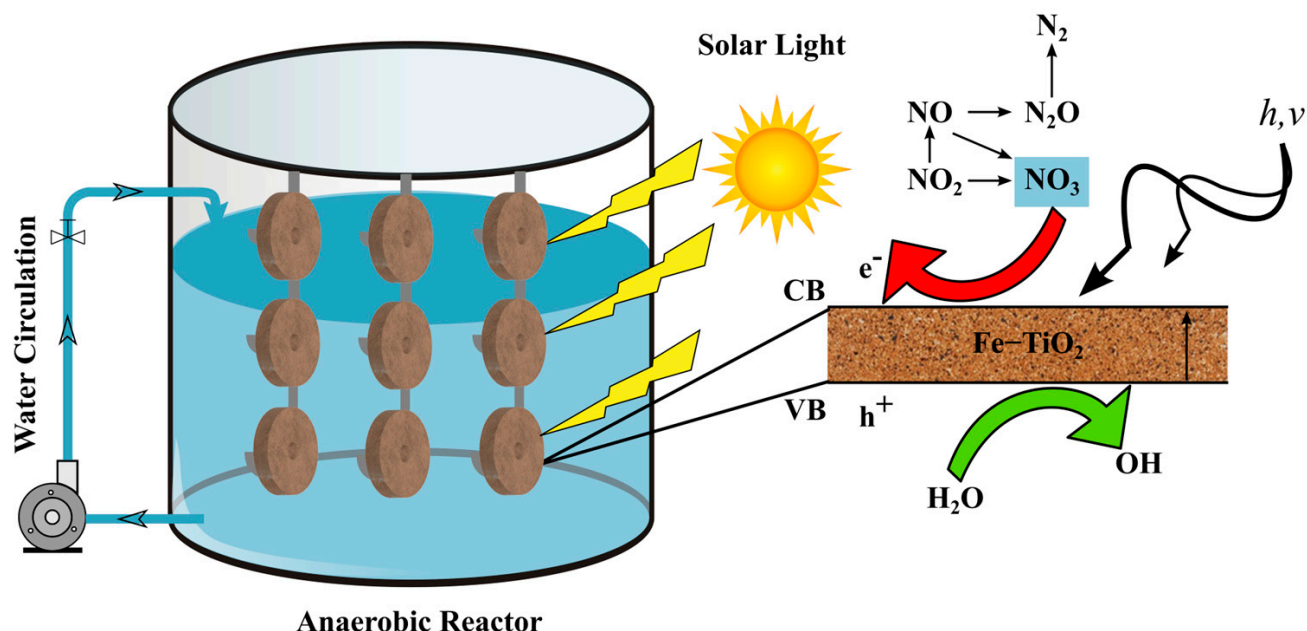


Figure 5. Proposed mechanism of the photocatalytic reduction of NO₃ using Fe-TiO₂-coated filters.

3. Materials and Methods

3.1. Materials and Chemicals

For the 3D printing mold, the 1.75 mm diameter polylactic acid (PLA) filament was bought from FLASHFORDGE 3D company, Los Angeles, CA, USA. Earthenware clay was acquired from the local pottery shop in Hyderabad, Pakistan. Titanium precursor salt titanium tetraisopropoxide (TTIP, $\text{Ti}[\text{OCH}(\text{CH}_3)_2]_4$, 97% purity), iron nitrate nonahydrate ($\text{Fe}(\text{NO}_3)_3 \cdot 9 \text{H}_2\text{O}$, 99.9% purity), 70% concentrated nitric acid (HNO_3), polyethylene glycol (PEG), and Triton-X were purchased from Sigma-Aldrich, Milan, Italy. The nitrate (NO_3^-) and nitrite (NO_2^-) titration pillows were purchased from a certified HACH supplier in Karachi, Pakistan. The indigo carmine (IC) dye (100% purity) was purchased from Acros Organics, Fisher Scientific, Waltham, MA, USA. All chemicals were used without further purification.

3.2. Synthesis of 3D Clay Filters

A 3D filter mold was designed and printed using Autodesk Fusion 360 software version 2.0.11186 and printed on a Flash Forge FDM 3D printer, Zhejiang, China using the previously reported method [22]. A mold with dimensions of 35 mm in diameter and 8 mm in thickness was used to give the clay filters a standard shape. The uniform and wetted dough of the collected earthenware clay was filled in the mold, allowed to dry, and later smoothly withdrawn and sun-dried in the 3D-structured filter shape. The dried filters were annealed in a muffle furnace, Carbolite Gero Company, Germany at 600 °C. Annealing improved the physical properties of clay filters, no powdery appearance was observed on its surfaces, and rough and porous 3D-structured clay filters were obtained [22].

3.3. Coatings of Fe-TiO₂

The 0.25 M TTIP was dissolved in 0.5 M solution of HNO_3 , and $\text{Fe}(\text{NO}_3)_3 \cdot 9\text{H}_2\text{O}$ was added at a nominal stoichiometric weight to obtain 2.5% of Fe in the resultant mixture. Afterward, a uniform sol–gel was prepared with non-ionic surfactant Triton X-100, adding 0.1 mL/10 mL for uniform dispersion, while 0.5 mL PEG per 1 mL/10 mL of the solution was added for improved polymerization of the resultant photocatalyst particles on the clay surface. For coatings, the annealed clay filters were impregnated and soaked in the produced sol–gel solution at the 15 mL/filter quantity for 1 h at room temperature. The completely soaked clay filters were treated in the muffle furnace at 150, 300, and 450 °C for 60, 45, and 90 min, respectively. A uniform thin layer of Fe-TiO₂ particles was achieved on the surface of the clay filter. The scheme of preparation of the sol–gel solution of Fe-TiO₂ particles and their coating on the synthesized 3D clay filter is shown in Figure 6. This method is repeated to produce and coat around 20 clay filters for the photocatalytic evaluation experiments.

3.4. Characterization Methods

The coated and uncoated filters and pristine anatase TiO₂ were characterized and analyzed at the DISAT laboratories, Politecnico di Torino, Italy. The FESEM images were acquired using the ZEISS MERLIN 4248 FESEM instrument (ZEISS MERLIN, Forchtenberg, Germany) i.e., to analyze the morphology of the bare and coated clay filters. Energy-dispersive X-ray spectroscopy (EDS, ZEISS MERLIN, Forchtenberg, Germany) was performed for the elemental analysis of the coated clay filter. Both filters' phase and crystalline structure were investigated using X-ray diffraction (XRD) using a Phillips X-ray diffractometer, Netherland (Phillips, Amsterdam, The Netherlands). The optical properties of the bare clay filter, coated clay filters, and pristine anatase TiO₂ (with Fe addition) were analyzed using a Varian Cary 500 spectrophotometer (Agilent, Santa Clara, CA, USA). The Tauc plot was adopted to determine the bare and coated clay filters' optical energy bandgap (E_g).

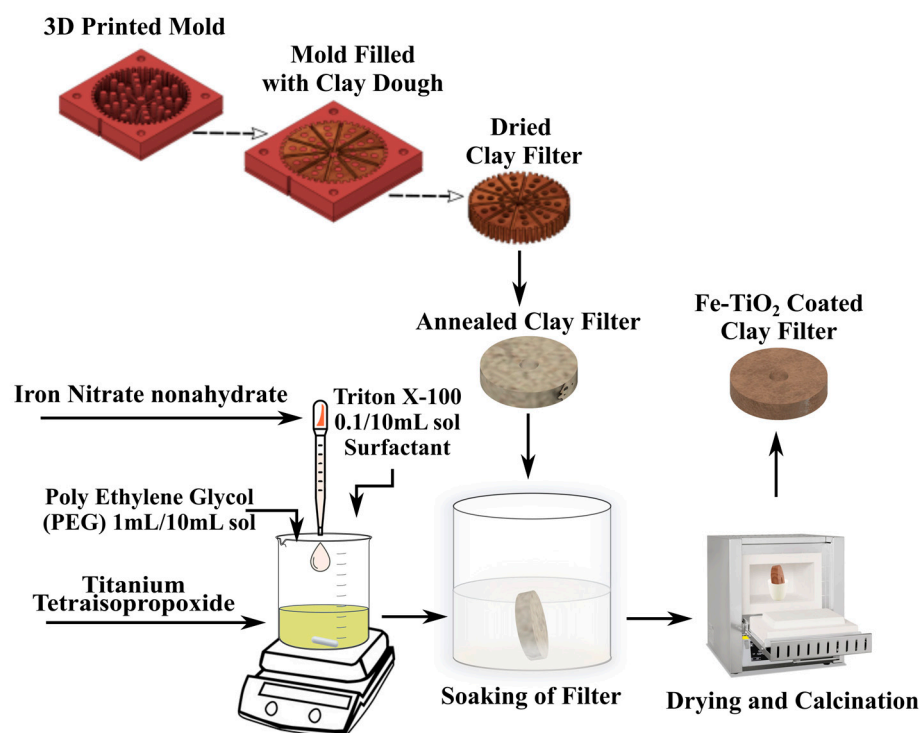


Figure 6. Schematic layout of the preparation of clay filters, precursor solution, and coating method.

3.5. Photocatalytic Activity of Fe-TiO₂ Clay Filters

Initially, the photocatalytic activity of coated clay filters was investigated for IC dye degradation under natural sunlight irradiation. For comparison, the bare clay filter was tested in the same sequence for any adsorption-based removal of IC dye (because clay has no reported photocatalytic properties). The photocatalytic test of pristine TiO₂ was not added to the experiment design because all of the experiments were planned under natural sunlight, and the reported performance of TiO₂ under natural or artificial sunlight is poor. A stock solution of 5 ppm IC dye concentration was produced. A small steel mesh assembly was fabricated to hold and diagonally lay down the clay filters in the beaker, i.e., exposed to sunlight under stirring at 300 rpm. The ratio of 1 mm/1 mL (filter diameter/dye solution volume) was adjusted. Three experiments were performed in different beakers i.e., a control (without any filter, only irradiation), dye solution and bare clay filters, and dye solution with Fe-TiO₂ clay filters, under natural sunlight irradiation during the daytime (11:00 a.m. to 3:00 p.m.). These experiments were performed outside the laboratory in Jamshoro city, Pakistan. The recorded ambient temperatures were in the range of 37 °C to 42 °C and the irradiation flux was in the range of 630–885 watts/m². During the experiment, the solution in beakers was stirred at a constant rpm, each containing 100 mL IC solution. The adsorption–desorption equilibrium was obtained by stirring solutions for 60 min in the dark, then sunlight irradiation was allowed and dye removal and degradation were observed at every 60 min interval until 180 min. A 2.5 mL aliquot was collected at each irradiation time interval, and a UV/Vis spectrophotometer was used to analyze the absorbance spectra of dye degradation [22]. The reduction of the main absorbance peak at 610 nm confirmed the photocatalytic degradation of IC dye using coated filters. The total organic carbon (TOC) analysis of the IC solution before and after photocatalytic tests was performed on the Shimadzu TOC analyzer (Shimadzu, Tokyo, Japan).

3.6. Nitrate Reduction Analysis

The results obtained from IC dye degradation revealed the efficient potential of Fe-TiO₂ clay filters, and then it was decided to analyze the photocatalytic reduction of NO₃ using bare clay filters and Fe-TiO₂ clay filters. A transparent glass batch-scale reactor with

a 3 L capacity was designed and configured for photocatalytic testing. The reactor scheme is displayed in Figure 5. The required filters were attached to the steel mesh assembly and diagonally positioned inside the reactor for maximum irradiation passage from the natural solar light.

Photocatalytic reduction of NO_3 was tested for a 2 L solution of 30, 50, and 100 ppm of NO_3 concentrations. Initially, the adsorption–desorption equilibrium was attained in dark conditions, and later, the reactor was exposed to natural sunlight irradiation. For solution agitation and maximum contact with the clay filters, a mini water circulating pump was connected to the inlet and outlet of the photocatalytic reactor and operated at a speed of 100 mL/min. The 2.5 mL aliquots were withdrawn from the reactor after 60, 120, 180, and 240 min intervals to analyze the NO_3 and NO_2^- concentrations using NO_3 and NO_2^- HACH buffer pillows and a DR900 spectrophotometer, HACH, Loveland, CO, USA [38]. The removal of NO_3 from the solution, i.e., before, during, and after the photocatalytic test, was analyzed using the Shimadzu total nitrogen (TN) analyzer.

4. Conclusions

The 3D-structured rough and porous clay filter was prepared using 3D printing and annealing techniques, in which the 3D-printed molds were designed and printed for molding and shaping the clay filters, i.e., before their annealing. The clay filters were successfully coated with Fe- TiO_2 round-shaped particles, i.e., following the soaking in sol–gel and calcination in the furnace at around 450 °C. Different analyses, such as XRD, UV/Vis DRS, and FESEM, confirmed the coatings of Fe- TiO_2 films on the tiny pores and channels of the 3D-structured clay filters and changes in the properties of pristine TiO_2 , i.e., due to the addition of nominal 2.5% Fe. The results obtained from the photocatalytic degradation of IC dye confirmed the photocatalytic performance and improved kinetics of the Fe- TiO_2 clay filter under natural sunlight. Afterward, the photocatalytic reduction of 30, 50, and 100 ppm NO_3 concentrations was validated using the Fe- TiO_2 -coated clay filter. The TN analysis and reduction of NO_3 to NO_2^- revealed the reduction of NO_3 owing to the induced photocatalytic response of the Fe- TiO_2 -coated clay filter with 81% removal of 30 ppm solution after 240 min of treatment. The NO_3 reduction path was studied by analyzing the transformation of NO_3 into NO_2 , NO , and N_2 . Overall, the presented results showed the potential of the 3D printing and Fe- TiO_2 clay filter to treat NO_3 and other related wastewater contaminants for large-scale applications.

Author Contributions: Conceptualization and methodology by T.A.G. Experimental protocol, synthesis, photocatalytic testing, and validation by I.A.B., T.A.Q. and A.L. Formal analysis and interpretation by T.A.G., N.C. and I.A. Data compilation and writing by I.A.B., T.A.Q., I.A. and T.A.G. Writing—review, revision, proofreading, and editing by T.A.G., R.B.M. and B.B. All authors have read and agreed to the published version of the manuscript.

Funding: This research received no external funding.

Data Availability Statement: Not applicable.

Acknowledgments: The authors acknowledge the technical support of Alberto Tagliaferro, Alessandro Chiadò, Paola Rivolo, and Mattia Bartoli from Politecnico di Torino, Italy, and Abdul Manan Memon from USPCASW, Mehran University of Engineering and Technology, Jamshoro.

Conflicts of Interest: The authors declare no conflict of interest.

References

1. Zhongming, Z.; Linong, L.; Xiaona, Y.; Wei, L. Half of global wastewater treated, rates in developing countries still lagging. *Earth Syst. Sci. Data* **2021**, *13*, 237–254.
2. Margot, J.; Rossi, L.; Barry, D.A.; Holliger, C. A review of the fate of micropollutants in wastewater treatment plants. *Wiley Interdiscip. Rev. Water* **2015**, *2*, 457–487. [[CrossRef](#)]
3. Sharif, M.; Jabbar, A.; Niazi, M.A.; Mahr, A.B. Managing water availability and requirements in Pakistan: Challenges and way forward. *J. Agric. Res.* **2016**, *54*, 117–131.

4. Thamdrup, B.; Dalsgaard, T. Production of N₂ through anaerobic ammonium oxidation coupled to nitrate reduction in marine sediments. *Appl. Environ. Microbiol.* **2002**, *68*, 1312–1318. [[CrossRef](#)] [[PubMed](#)]
5. Wang, J.H.; Baltzis, B.; Lewandowski, G. Reduction of nitrate and nitrite in a cyclically operated continuous biological reactor. *Biotechnol. Bioeng.* **1995**, *46*, 159–171. [[CrossRef](#)]
6. Rodríguez, D.C.; Pino, N.; Peñuela, G. Monitoring the removal of nitrogen by applying a nitrification–denitrification process in a Sequencing Batch Reactor (SBR). *Bioresour. Technol.* **2011**, *102*, 2316–2321. [[CrossRef](#)]
7. Oka, M.; Miseki, Y.; Saito, K.; Kudo, A. Photocatalytic reduction of nitrate ions to dinitrogen over layered perovskite BaLa₄Ti₄O₁₅ using water as an electron donor. *Appl. Catal. B Environ.* **2015**, *179*, 407–411. [[CrossRef](#)]
8. Daud, M.; Nafees, M.; Ali, S.; Rizwan, M.; Bajwa, R.A.; Shakoor, M.B.; Arshad, M.U.; Chatha, S.A.S.; Deeba, F.; Murad, W. Drinking water quality status and contamination in Pakistan. *BioMed. Res. Int.* **2017**, *2017*, 7908183. [[CrossRef](#)]
9. Zhang, Y.; Li, F.; Zhang, Q.; Li, J.; Liu, Q. Tracing nitrate pollution sources and transformation in surface-and ground-waters using environmental isotopes. *Sci. Total Environ.* **2014**, *490*, 213–222. [[CrossRef](#)]
10. Zhang, D.; Wang, B.; Gong, X.; Yang, Z.; Liu, Y. Selective reduction of nitrate to nitrogen gas by novel Cu₂O-Cu⁰@Fe⁰ composite combined with HCOOH under UV radiation. *Chem. Eng. J.* **2019**, *359*, 1195–1204. [[CrossRef](#)]
11. Pinto, H.B.; de Souza, B.M.; Dezotti, M. Treatment of a pesticide industry wastewater mixture in a moving bed biofilm reactor followed by conventional and membrane processes for water reuse. *J. Clean. Prod.* **2018**, *201*, 1061–1070. [[CrossRef](#)]
12. Cai, C.; Hu, S.; Guo, J.; Shi, Y.; Xie, G.-J.; Yuan, Z. Nitrate reduction by denitrifying anaerobic methane oxidizing microorganisms can reach a practically useful rate. *Water Res.* **2015**, *87*, 211–217. [[CrossRef](#)]
13. de Bem Luiz, D.; Andersen, S.L.F.; Berger, C.; José, H.J.; Moreira, R.d.F.P.M. Photocatalytic reduction of nitrate ions in water over metal-modified TiO₂. *J. Photochem. Photobiol. A Chem.* **2012**, *246*, 36–44. [[CrossRef](#)]
14. Shaban, Y.A.; El Maradny, A.A.; Al Farawati, R.K. Photocatalytic reduction of nitrate in seawater using C/TiO₂ nanoparticles. *J. Photochem. Photobiol. A Chem.* **2016**, *328*, 114–121. [[CrossRef](#)]
15. Li, Y.; Wasgestian, F. Photocatalytic reduction of nitrate ions on TiO₂ by oxalic acid. *J. Photochem. Photobiol. A Chem.* **1998**, *112*, 255–259. [[CrossRef](#)]
16. Kobwittaya, K.; Sirivithayapakorn, S. Photocatalytic reduction of nitrate over TiO₂ and Ag-modified TiO₂. *J. Saudi Chem. Soc.* **2014**, *18*, 291–298. [[CrossRef](#)]
17. Litter, M.; Navio, J.A. Photocatalytic properties of iron-doped titania semiconductors. *J. Photochem. Photobiol. A Chem.* **1996**, *98*, 171–181. [[CrossRef](#)]
18. Ali, T.; Tripathi, P.; Azam, A.; Raza, W.; Ahmed, A.S.; Ahmed, A.; Muneer, M. Photocatalytic performance of Fe-doped TiO₂ nanoparticles under visible-light irradiation. *Mater. Res. Express* **2017**, *4*, 015022. [[CrossRef](#)]
19. Freyria, F.S.; Compagnoni, M.; Ditaranto, N.; Rossetti, I.; Piumetti, M.; Ramis, G.; Bonelli, B. Pure and Fe-doped mesoporous titania catalyse the oxidation of acid orange 7 by H₂O₂ under different illumination conditions: Fe doping improves photocatalytic activity under simulated solar light. *Catalysts* **2017**, *7*, 213. [[CrossRef](#)]
20. Tugaoen, H.O.N.; Garcia-Segura, S.; Hristovski, K.; Westerhoff, P. Challenges in photocatalytic reduction of nitrate as a water treatment technology. *Sci. Total Environ.* **2017**, *599*, 1524–1551. [[CrossRef](#)]
21. Mukhopadhyay, R.; Bhaduri, D.; Sarkar, B.; Rusmin, R.; Hou, D.; Khanam, R.; Sarkar, S.; Biswas, J.K.; Vithanage, M.; Bhatnagar, A. Clay–polymer nanocomposites: Progress and challenges for use in sustainable water treatment. *J. Hazard. Mater.* **2020**, *383*, 121125. [[CrossRef](#)] [[PubMed](#)]
22. Latif, A.; Memon, A.M.; Gadhi, T.A.; Bhurt, I.A.; Channa, N.; Mahar, R.B.; Ali, I.; Chiadò, A.; Bonelli, B. Bi₂O₃ immobilized 3D structured clay filters for solar photocatalytic treatment of wastewater from batch to scaleup reactors. *Mater. Chem. Phys.* **2022**, *276*, 125297. [[CrossRef](#)]
23. Lazaratou, C.; Vayenas, D.; Papoulis, D. The role of clays, clay minerals and clay-based materials for nitrate removal from water systems: A review. *Appl. Clay Sci.* **2020**, *185*, 105377. [[CrossRef](#)]
24. Dommati, H.; Ray, S.S.; Wang, J.-C.; Chen, S.-S. A comprehensive review of recent developments in 3D printing technique for ceramic membrane fabrication for water purification. *RSC Adv.* **2019**, *9*, 16869–16883. [[CrossRef](#)]
25. Shah, L.A.; da Silva Valenzuela, M.d.G.; Farooq, M.; Khattak, S.A.; Díaz, F.R.V. Influence of preparation methods on textural properties of purified bentonite. *Appl. Clay Sci.* **2018**, *162*, 155–164. [[CrossRef](#)]
26. Akowanou, A.V.O.; Deguenon, H.E.J.; Groendijk, L.; Aina, M.P.; Yao, B.K.; Drogui, P. 3D-printed clay-based ceramic water filters for point-of-use water treatment applications. *Prog. Addit. Manuf.* **2019**, *4*, 315–321. [[CrossRef](#)]
27. Gogoi, J.; Choudhury, A.D.; Chowdhury, D. Graphene oxide clay nanocomposite as an efficient photo-catalyst for degradation of cationic dye. *Mater. Chem. Phys.* **2019**, *232*, 438–445. [[CrossRef](#)]
28. Addamo, M.; Augugliaro, V.; Di Paola, A.; García-López, E.; Loddo, V.; Marci, G.; Palmisano, L. Photocatalytic thin films of TiO₂ formed by a sol–gel process using titanium tetraisopropoxide as the precursor. *Thin Solid Film.* **2008**, *516*, 3802–3807. [[CrossRef](#)]
29. Kapridaki, C.; Xynidis, N.; Vazgiouraki, E.; Kallithrakas-Kontos, N.; Marvelaki-Kalaitzaki, P. Characterization of photoactive Fe-TiO₂ lime coatings for building protection: The role of iron content. *Materials* **2019**, *12*, 1847. [[CrossRef](#)]
30. Aranda, P.; Ruiz-Hitzky, E. Immobilization of nanoparticles on fibrous clay surfaces: Towards promising nanoplatforms for advanced functional applications. *Chem. Rec.* **2018**, *18*, 1125–1137. [[CrossRef](#)]
31. Barka, N.; Assabane, A.; Nounah, A.; Ichou, Y.A. Photocatalytic degradation of indigo carmine in aqueous solution by TiO₂-coated non-woven fibres. *J. Hazard. Mater.* **2008**, *152*, 1054–1059. [[CrossRef](#)] [[PubMed](#)]

32. Hernández-Gordillo, A.; Bizarro, M.; Gadhi, T.A.; Martínez, A.; Tagliaferro, A.; Rodil, S.E. Good practices for reporting the photocatalytic evaluation of a visible-light active semiconductor: Bi₂O₃, a case study. *Catal. Sci. Technol.* **2019**, *9*, 1476–1496. [[CrossRef](#)]
33. Gadhi, T.A.; Mahar, R.B.; Bonelli, B. Actual mineralization versus partial degradation of wastewater contaminants. In *Nanomaterials for the Detection and Removal of Wastewater Pollutants*; Elsevier: Amsterdam, The Netherlands, 2020; pp. 331–350.
34. Gadhi, T.A.; Hernández-Gordillo, A.; Bizarro, M.; Jagdale, P.; Tagliaferro, A.; Rodil, S.E. Efficient α/β -Bi₂O₃ composite for the sequential photodegradation of two-dyes mixture. *Ceram. Int.* **2016**, *42*, 13065–13073. [[CrossRef](#)]
35. Sandhu, S.; Krishnan, S.; Karim, A.V.; Shrivastav, A. Photocatalytic denitrification of water using polystyrene immobilized TiO₂ as floating catalyst. *J. Environ. Chem. Eng.* **2020**, *8*, 104471. [[CrossRef](#)]
36. Huang, R.; Liang, R.; Fan, H.; Ying, S.; Wu, L.; Wang, X.; Yan, G. Enhanced photocatalytic fuel denitrification over TiO₂/ α -Fe₂O₃ nanocomposites under visible light irradiation. *Sci. Rep.* **2017**, *10*, 7858. [[CrossRef](#)]
37. Lin, Z.Q.; Yuan, S.J.; Li, W.W.; Chen, J.J.; Sheng, G.P.; Yu, H.Q. Denitrification in an integrated bioelectro-photocatalytic system. *Water Res.* **2017**, *1*, 88–93. [[CrossRef](#)]
38. Maghanga, J.; Kituyi, J.; Kisinyo, P.; Ng'Etich, W. Impact of nitrogen fertilizer applications on surface water nitrate levels within a Kenyan tea plantation. *J. Chem.* **2013**, *2013*, 196516. [[CrossRef](#)]

Disclaimer/Publisher's Note: The statements, opinions and data contained in all publications are solely those of the individual author(s) and contributor(s) and not of MDPI and/or the editor(s). MDPI and/or the editor(s) disclaim responsibility for any injury to people or property resulting from any ideas, methods, instructions or products referred to in the content.